A New Chronology of Late Quaternary Sequences From the Central Arctic Ocean Based on "Extinction Ages" of Their Excesses in 231 Pa and 230 Th

C. Hillaire-Marcel, B. Ghaleb, A. de Vernal, J. Maccali, K. Cuny, A. Jacobel, C. Le Duc, J. Mcmanus

AGU PUBLICATIONS

Geochemistry, Geophysics, Geosystems

RESEARCH ARTICLE
10.1002/2017GC007050

Special Section:
The Arctic: An AGU Joint Special Collection

A New Chronology of Late Quaternary Sequences From the Central Arctic Ocean Based on "Extinction Ages" of Their Excesses in ^{231}Pa and ^{230}Th

C. Hillaire-Marcel[1], B. Ghaleb[1], A. de Vernal[1], J. Maccali[1], K. Cuny[2], A. Jacobel[3], C. Le Duc[1], and J. McManus[3]

[1]GEOTOP, Université du Québec à Montréal, Montréal, QC, Canada, [2]Laboratoire des Sciences du Climat et de l'Environnement, Gif-sur-Yvette, France, [3]Department of Earth and Environmental Sciences, Columbia University Lamont-Doherty Earth Observatory, Palisades, NY, USA

Abstract Merging the late Quaternary Arctic paleoceanography into the Earth's global climate history remains challenging due to the lack of robust marine chronostratigraphies. Over ridges notably, low and variable sedimentation rates, scarce biogenic remains ensuing from low productivity and/or poor preservation, and oxygen isotope and paleomagnetic records differing from global stacks represent major impediments. However, as illustrate here based on consistent records from Mendeleev-Alpha and Lomonosov Ridges, disequilibria between U-series isotopes can provide benchmark ages. In such settings, fluxes of the particle-reactive U-daughter isotopes ^{230}Th and ^{231}Pa from the water column, are not unequivocally linked to sedimentation rates, but rather to sea-ice rafting and brine production histories, thus to the development of sea-ice factories over shelves during intervals of high relative sea level. The excesses in ^{230}Th and ^{231}Pa over fractions supported by their parent U-isotopes, collapse down sedimentary sequences, due to radioactive decay, and provide radiometric benchmark ages of approximately 300 and 140 ka, respectively. These "extinction ages" point to mean sedimentation rates of ~4.3 and ~1.7 mm/ka, respectively, over the Lomonosov and Mendeleev Ridges, which are significantly lower than assumed in most recent studies, thus highlighting the need for revisiting current interpretations of Arctic lithostratigraphies in relation to the global-scale late Quaternary climatostratigraphy.

Plain Language Summary The Arctic Ocean represents a major component of the Earth climate system notably with regard to the Arctic amplification and freshwater fluxes toward the global ocean. Understanding its role versus the global climate history of the recent glacial/interglacial cycles remains challenging due to the lack of robust chronology of marine sedimentary archives. In the present study, we demonstrate that the decay of Uranium series isotopes in sediments from major Arctic ridges provide benchmark ages for the last ~300,000 years and support the concept of a "sediment-starved" environment in the central Arctic Ocean.

Key Points:
- New chronology of late Quaternary marine sequences from the central Arctic
- Mean sedimentation rates of the order of millimeters per thousand years over ridges
- Highly discontinuous ice-rafted sedimentation over ridges with gaps

Supporting Information:
- Supporting Information S1
- Table S1
- Table S2
- Table S3
- Table S4
- Table S5
- Table S6
- Figure S1
- Figure S2
- Figure S3
- Figure S4

Correspondence to:
C. Hillaire-Marcel,
chm@uqam.ca

Citation:
Hillaire-Marcel, C., Ghaleb, B., de Vernal, A., Maccali, J., Cuny, K., Jacobel, A., . . . McManus, J. (2017). A new chronology of late quaternary sequences from the central Arctic Ocean based on "extinction ages" of their excesses in ^{231}Pa and ^{230}Th. *Geochemistry, Geophysics, Geosystems*, *18*, 4573–4585. https://doi.org/10.1002/2017GC007050

Received 6 JUN 2017
Accepted 16 NOV 2017
Accepted article online 4 DEC 2017
Published online 26 DEC 2017

1. Introduction

The Arctic Ocean represents a major component of the Earth climate system notably with regard to Arctic amplification and freshwater budget (e.g., CliC/AMAP/IASC, 2016; Serreze & Francis, 2006). However, its role in the climate history of the late Cenozoic remains speculative due to the lack of unquestionable chronostratigraphies especially on glacial/interglacial time scales. Anchoring stratigraphies to the Brunhes/Matuyama transition, pioneering work by Clark et al. (1980) led to the conclusion that the central Arctic Ocean was a "sediment-starved" region with sedimentation rates of the order of a few mm/ka. Similarly, research based on U-series isotopes by Ku and Broecker (1967) and Huh et al. (1989), supported such low sedimentation rates as did several studies of the 80s (e.g., Aksu & Mudie, 1985). Later on, however, new attempts at setting detailed chronology of late Quaternary sequences were made using chronostratigraphic tools such as optically stimulated luminescence, stable isotopes in foraminifers, Mn-layer counts and cyclostratigraphy, paleomagnetic excursions, and site to site correlations across the Arctic Ocean (cf. Backman et al., 2004; Jakobsson et al., 2000, 2001, 2003; Löwemark et al., 2014; O'Regan et al., 2008). On these bases, significantly higher sedimentation rates than those proposed earlier were hypothesized and a late

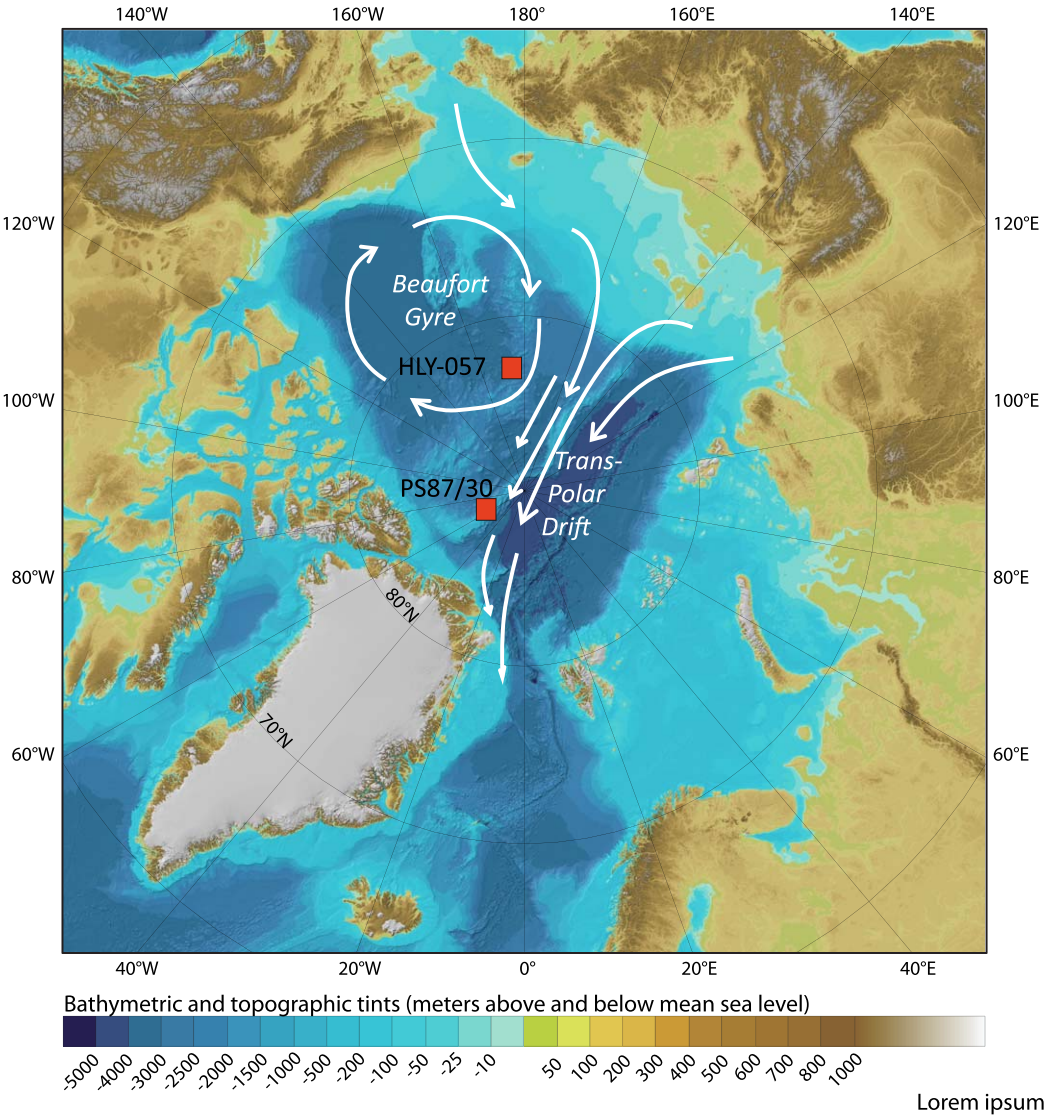

Figure 1. Location map of cited features and coring sites. Background map from Jakobsson et al. (2012). White arrows indicate major sea-ice rafting routes.

Quaternary history of the Arctic Ocean was tentatively integrated into hemispheric paleoclimate schemes (cf. Cronin et al., 2014; Polyak et al., 2013; Stein, 2015). More recently, geochemical studies using ^{10}Be (Sellén et al., 2009) and U-series isotopes (Not & Hillaire-Marcel, 2010) led to conclude that sedimentation rates were likely close to those originally estimated by Clark et al. (1980) or Huh et al. (1997). Here, we intend to demonstrate that the approach developed by Not and Hillaire-Marcel (2010) for setting benchmark radiometric ages in late Quaternary sequences, based on the decay of ^{230}Th and ^{231}Pa excesses through time, can be also applied to low sedimentation rate sites of the Lomonosov Ridge (Figure 1).

Since the late 80s, much work has been done concerning the behavior of particle-reactive U-daughter isotopes in the Arctic Ocean and its sediments. Studies range from investigations on the distribution ^{231}Pa and ^{230}Th in the water column (e.g., Bacon et al., 1989; Cochran et al., 1995; Scholten et al., 1995; Trimble et al., 2004), with attention paid to their fractionation in relation to particulate fluxes (e.g., Edmonds et al., 2004), to the documenting of their behavior through time from sediment analysis (e.g., Hoffmann et al., 2013; Huh et al., 1997; Somayajulu et al., 1989). A concise and up-do-date summary of these findings can be found in Hoffmann et al.'s paper (2013). This paper also documents some decrease of ^{231}Pa/^{230}Th ratios with water depth, as well as back in time from the Holocene to the Last Glacial Maximum. Aside from showing features

similar to those illustrated in Hoffmann et al. (2013), the present study does not address specifically the cycling of these isotopes in the Arctic Ocean, although it leads to suggest a mechanism linked to sea-ice production for their scavenging. It mostly aims at testing the applicability of the ^{231}Pa/^{230}Th-based method proposed by Not and Hillaire-Marcel (2010), following early work by Huh et al. (1997) and Somayajulu et al. (1989), for the setting of robust benchmark ages in low sedimentation rate sites of central Arctic Ocean ridges. As will be demonstrated, results from both the Northern Mendeleev Ridge (Not & Hillaire-Marcel, 2010) and Lomonosov Ridge (present study) concur to support the concept of a "sediment-starved" environment in the central Arctic Ocean. From a geochemical viewpoint, they point to scavenging mechanisms of the ^{231}Pa and ^{230}Th produced by dissolved U in the water column specific to the sea-ice environment and history of the Arctic Ocean.

2. Sediment Cores, Sampling, and Analyses

The study site is located in the central part of the Lomonosov Ridge (Figure 1). It was cored during Polarstern expedition PS87 in 2014 (Stein, 2015). We use here a multicore (PS87/030-3; 88°39.39′N, 61° 25.55′W; water depth 1277.8 m) and the Karstenlot core, raised a few cables apart (PS87/030-1; 88°39.72′N, 61°32.52′W; water depth 1276.8 m), henceforth named MC-030 and K-030, respectively. Both cores were sampled continuously at 1 cm intervals down to 11.5 cm (MC-030) or 12.5 cm (K-030). Below 12.5 cm, core K-030 was sampled at ~4 cm intervals down to 147.25 cm and at ~10 cm intervals, down to 258 cm. The sediment consists mostly of mean silt-size mud layers alternating with coarser sand-rich muds, with a few cm thick intervals rich in biogenic carbonates (Stein, 2015; Zwick, 2016). At the core top, the largest biogenic remains (otoliths and mollusk shells) were often covered by Mn-Fe coating.

All MC-030 samples collected at 1 cm interval were analyzed, whereas 1 cm thick samples were selected in K-030 at variable depths (see supporting information Table S3). The analytical results presented here generally include laser-grain size measurements, X-ray mineralogy, ^{210}Pb activities by alpha and/or gamma counting, U-series and Th-series abundances and/or molar and activity ratios (^{232}Th, ^{238}U, ^{234}U, ^{230}Th, ^{226}Ra, ^{231}Pa) from ICPMS measurements (^{231}Pa/^{230}Th) or MC-ICP-MS measurements (all other isotopes) and AMS-^{14}C dating of *Neogloboquadrina pachyderma* (Np) shells (see supporting information for the description of analytical techniques and reproducibility; supporting information Tables S1–S5). In order to link K-030 core top to MC-030, ^{210}Pb measurements were also performed at 1 cm intervals in K-020 down to 12.5 cm. Complementary results (inorganic and organic carbon contents, organic C/total N ratio, δ^{13}C-organic C) are available upon request.

Radiocarbon dates were converted into calibrated ages using the Blaauw and Christen's Bacon software for depth/age modeling (Blaauw & Christen, 2011). A marine "reservoir age" $\Delta R = 440$ years has been used, prior to conversion, based on pre-Suess effect ^{14}C-data from the Canadian Arctic margin (cf. Calib 7; Reimer & Reimer, 2001). Through time, this value has probably changed (Hanslik et al., 2010), but the mean sedimentation rate estimate obtained from ages calibrated in this way should be relatively robust.

U-series isotope concentrations were converted into activities using half-lives from Cheng et al. (2000) for U and Th isotopes, and from Robert et al. (1969), for ^{231}Pa. Results are quoted either with one standard deviation (grain size, ^{210}Pb activity) or 2 standard deviations (calibrated ages, U, Th, and Pa isotopes), whereas a relative uncertainty of about ±5% (±1σ) is estimated for the semiquantitative X-ray mineralogical results and grain size measurements (see supporting information S1, Baskaran & Naidu, 1995; Blaauw & Christen, 2011; Blott & Pye, 2001; Cheng et al., 2000; Fleisher & Anderson, 2003; Kraus et al., 1956, Martin-Ramos et al., 2012; Not et al., 2008; Pons-Branchu et al., 2005; Thorez, 2003).

3. Results

The sedimentary sequence of core K-030 consists of silty to sandy sediments, with a few larger clasts. The mean grain size varies from ~8 to ~60 μm, with an average value of 24 ± 14 μm (supporting information Table S6). Silty-dominated layers (mean size < 15 μm), containing microfaunal remains, alternate with sand-rich layers (mean size > 20 μm; 15% < sand < 40% of total sediment) deprived of biogenic remains (see also Zwick, 2016), suggesting variable ice-rafting depositional processes at their origin depending sea-ice versus iceberg dominated drifting. Clay and sand contents are anticorrelated ($R = -0.78$; see supporting

information Table S6). The mineralogical composition includes quartz (~40%), feldspars (~31%), micas (~14%), and Fe-clinochlore (~13%), with variable traces of calcite, dolomite, halite, mangano-calcite, amphibolites, magnetite, hematite, and interstratified clays. Contrary to the northern Mendeleev Ridge where detrital carbonates (dolomite + calcite) could sum up to nearly 50% (Not & Hillaire-Marcel, 2010), they rarely exceed a few percent at the study site, except at 80 cm downcore K-030 where they reach 13%. Dolomite, thought to label detrital sources from Arctic Canada (e.g., Bischof et al., 1996; Darby et al., 2002; Polyak et al., 2004), never exceeds 1.4% in the study cores.

Lead-210 data (see supporting information Tables S2 and S3) were used to correlate MC-030 and K-030. They indicate the loss of about 3 cm on top of the Kastenlot core and record minor differences in sedimentation rates and/or some discrete compaction, but depict overall nearly similar patterns. Based on this correlation, a composite record was set up for the calculation of inventories of ^{231}Pa and ^{230}Th excesses, over their parent isotopes, at the site. The ^{210}Pb distribution in MC-030 is similar to that of the Mendeleev Ridge (Not et al., 2008). The excess in ^{210}Pb over parent ^{226}Ra is restricted to the upper 2.5 cm (versus about 1 cm in Mendeleev Ridge). Below and down to ~7 cm, ^{210}Pb follows closely the ^{226}Ra diffusive gradient toward bottom water. Deeper downcore, both ^{210}Pb and ^{226}Ra follow the ^{230}Th distribution, but for some minor diffusion of ^{226}Ra (mimicked by ^{210}Pb) on both sides of the ^{230}Th peaks. This pattern is characteristic of sites with very low sedimentation rates allowing the development of a strong ^{226}Ra-diffusion gradient below sediment surface, with ^{210}Pb-excess distribution being generally governed by shallow benthic mixing, as indicated by the ^{14}C-age of this layer (see below and also Not et al. (2008)).

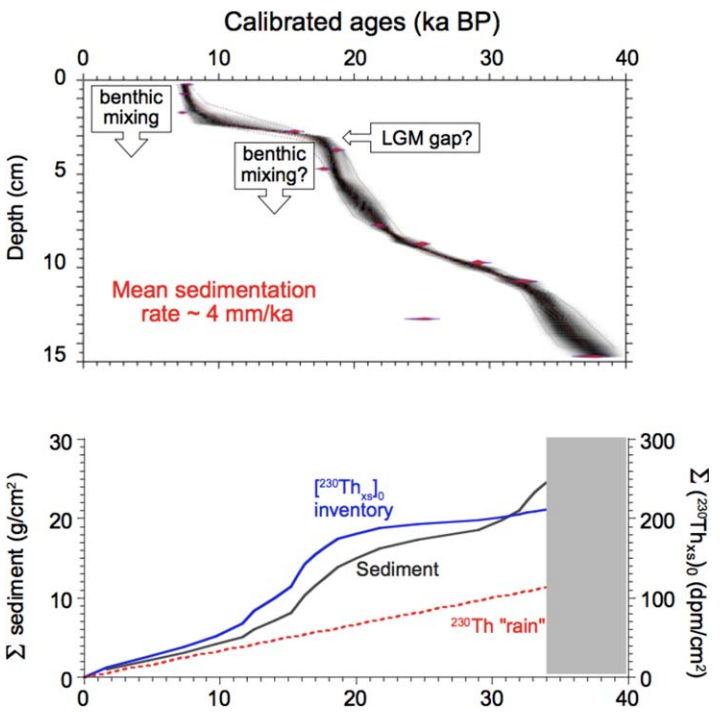

Figure 2. (a) Age model in MC-030 from Lomonosov Ridge (using BACON R440 from Blaauw and Christen (2011)). A marine "reservoir age" $\Delta R = 440$ years has been used, prior to conversion, based on pre-Suess effect ^{14}C-data from the Canadian Arctic margin (cf. Calib 7; Reimer & Reimer, 2001). Note that layers such as the 0–2 and 3–5 cm are likely fully mixed layers due to benthic mixing, as illustrated by similar ^{14}C ages at their top and bottom, thus leading to artificial time spans when fed into the Bacon software. Nevertheless, a first-order estimate of ~4 mm/ka can be retained for the mean sedimentation rate over the ca 40 ka interval recorded in the multicore. (b) Cumulative curves of sediment and of $\Sigma(^{230}Th_{xs})_0$ (i.e., initial excesses in ^{230}Th corrected for radioactive decay since deposition) in core MC-030, based on the above age model. $\Sigma(^{230}Th_{xs})_0$ exceeds considerably the ^{230}Th production in the overlying water column during the same time interval (see also Hoffmann & McManus, 2007); both accumulation curves depict overall similar variations, except near core bottom, where time control is not well constrained.

Calibrated ages from radiocarbon measurements in layers with sufficient *Neogloboquadrina pachyderma* (Np) tests yield the age-depth distribution illustrated in Figure 2. A mean sedimentation rate of about 4 mm/ka can be estimated for the last ~40 ka, but with large amplitude variations. The Holocene barely reaches 2 mm/ka as benthic mixing over about 2.5 cm should be largely responsible for the observed nearly constant ^{14}C-ages at core top. This is confirmed by the ^{210}Pb-excess over ^{226}Ra, down to the same depth, as described above. The mean calibrated ^{14}C-age of this mixed layer (~8 ka) is similar to that observed at other sites of the central Arctic, in particular in the northern Mendeleev Ridge sequences (Not & Hillaire-Marcel, 2010). It suggests maximum biogenic production during the early Holocene. Downcore, clusters of ^{14}C ages may also indicate earlier short intervals with biogenic productivity and benthic mixing over a couple of centimeters (Figure 2). In contradistinction, some intervals have barely left any sedimentary record at all. This is the case of the last glacial maximum, which is marked by a hiatus here (Figure 2a) as well as in records from Mendeleev Ridge records (Not & Hillaire-Marcel, 2010) and several other sites of the central Arctic Ocean (e.g., Nørgaard-Pedersen et al., 2003). In such records, correlation between grain size and/or sand content with interpolated sedimentation rates from dated layers is equivocal. Thus, even if the ^{14}C chronology provides here some constraints on sedimentation rates since ~40 ka BP, interpolations between dated layers may be misleading as such sedimentary sequences record discontinuous time intervals of highly variable duration, with unconstrained hiatuses.

Concentrations in U and Th (Figures 3 and 4 and supporting information Figures S1–S3) show little variation downcore. This suggests an overall low variability in detrital supply sources, in contrast to what was observed in Mendeleev Ridge sequences, where detrital carbonate peaks resulted in inversely proportional ^{232}Th-contents (Not & Hillaire-Marcel, 2010). In cores MC-030 and K-030, the [Th]/[U] molar ratio averages 5.26 ± 1.59 (±1σ), a value above the mean lithosphere

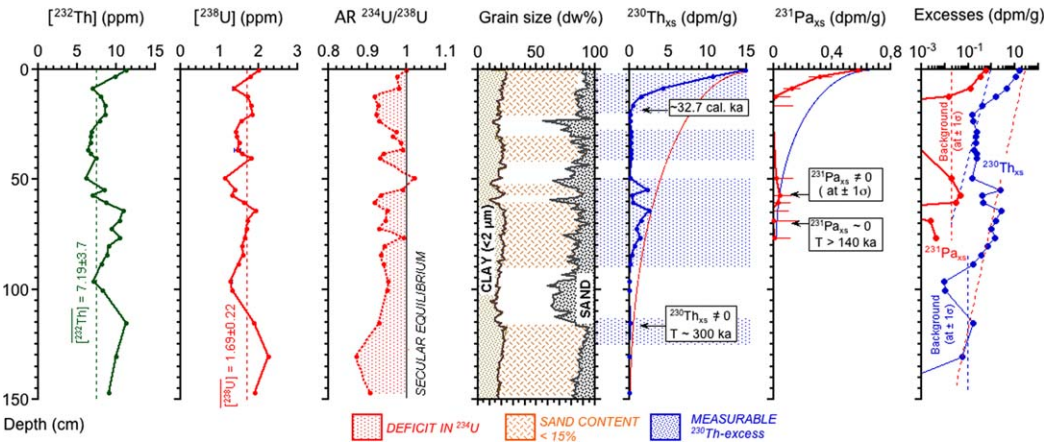

Figure 3. Overview of a few geochemical and sedimentological properties in core K-030 from the northern Lomonosov Ridge: Th and U contents, $^{234}U/^{238}U$ activity ratio, grain size distribution and its linkage with measurable excesses in ^{230}Th versus ^{238}U, measurable excesses in ^{231}Pa versus ^{235}U, chronological and stratigraphic interpretation of the extinction ages of excesses in both isotopes. Note the ^{230}Th and ^{231}Pa excesses restricted to layers with less than 15% of sand fraction. On the right, a log-plot of these excesses versus their 2σ uncertainty estimates versus fractions supported, respectively, by ^{238}U and ^{235}U (cf. "background" values).

composition but compatible within error bars with the composition of particulate matter from Russian rivers flowing into the Arctic (Th/U molar ratio ~4 (Viers et al., 2009)). One striking feature of the record is the relatively quite "flat" ^{238}U profile downcore that points to the absence or negligible diagenetic uranium addition or uranium mobility downcore. The deficit in ^{234}U versus ^{238}U in the study core (Figures 3 and 4 and supporting information Table S3) confirms the unlikeliness of U-addition, considering the $^{234}U/^{238}U$ activity ratio of 1.1434 ± 0.0036 of Arctic Ocean waters (Not et al., 2012). Instead, it points to U-losses with preferential departure of ^{234}U, either during the earlier continental cycling and transport of sedimentary particles (e.g., DePaolo et al., 2006; Ovaskainen, 1999), or following sedimentation due to the relatively oxidizing conditions at sea floor, which leads to the deposition of Mn-Fe oxide/hydroxide coatings (e.g., MacDonald & Gobeil, 2011). As in situ diagenetic U-losses would lead to uncertainties when estimating daughter ^{230}Th and ^{231}Pa excesses versus initial supported fractions in the sediment, this aspect will be discussed further below. The ^{230}Th and ^{231}Pa excesses illustrated in Figures 3 and 5 were simply calculated assuming the supported fractions of ^{230}Th and ^{231}Pa being equivalent to those of ^{238}U and ^{235}U, respectively, using the $^{238}U/^{235}U$ molar ratio value (137.818 ± 0.045; Hiess et al., 2012) to derive ^{235}U activities and concentrations from those of ^{238}U.

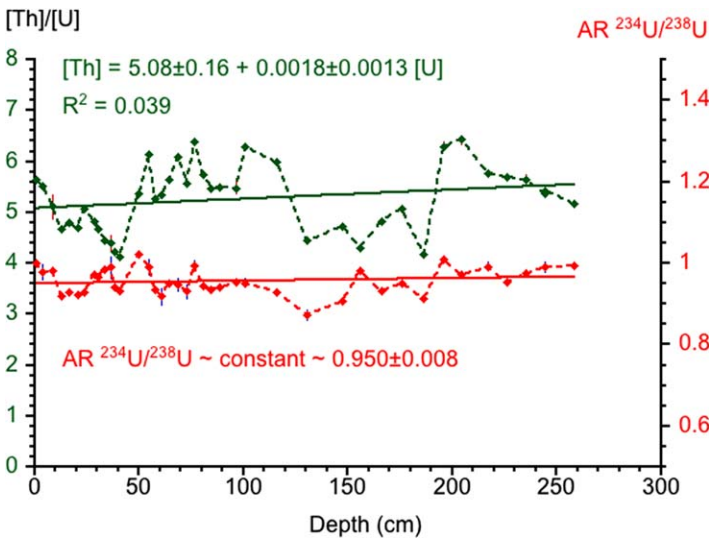

Figure 4. Molar ratio [Th]/[U] and activity ratio $^{234}U/^{238}U$ downcore K-030. Some variability in [Th] and [U] concentrations is observed in relation with lithological changes, but the $^{234}U/^{238}U$ activity ratio varies much less and depicts a nearly constant value throughout the sequence (see text).

Whatever the initial values of ^{230}Th and ^{231}Pa excesses (henceforth $^{230}Th_{xs}$, $^{231}Pa_{xs}$), they result from ^{230}Th and ^{231}Pa production by dissolved U decay in the water column. Being particle reactive, these isotopes are rapidly scavenged by particulate and/or colloidal matter, with some relative fractionation in the water column to be discussed later (Guo et al., 2002; Siddall et al., 2005). At the study site, as illustrated in Figure 3, $^{230}Th_{xs}$ and $^{231}Pa_{xs}$ are found exclusively in layers with a low sand content (<15%) and correlatively higher silt-clay contents. $^{230}Th_{xs}$ and $^{231}Pa_{xs}$ also depict a decay through time, deeper in the core, with residual values falling within error bars of their estimated supported fractions at depths of ~140 and ~60 cm downcore, respectively.

4. Discussion

4.1. The Calibrated ^{14}C Chronology and Its Limitation

At site PS87/30, a relatively robust ^{14}C chronology has been obtained (Figure 2a). It spans the last 35 ka. However, this chronology is partly

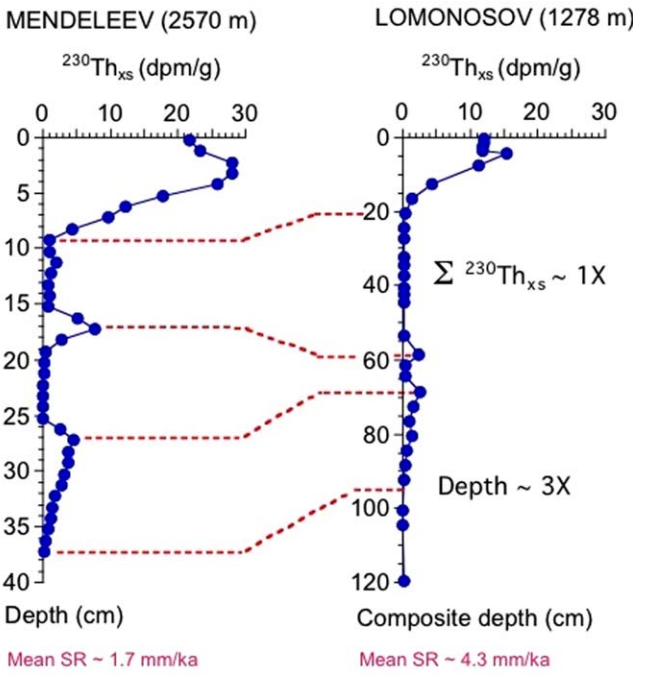

Figure 5. ^{230}Th-excess profiles in the composite Lomonosov core 030 (supporting information) versus the Mendeleev Ridge core MC-11 (Not & Hillaire-Marcel, 2010). Aside a very similar shape of both profiles, the comparison points to a ~3-fold higher mean sedimentation rate over Lomonosov versus Mendeleev. However, inventories of ^{230}Th-excesses in both cores are almost identical despite a more than 1.2 km difference in their bathymetry, raising the issue of an unusual ^{230}Th-cycling in the central Arctic Ocean.

floating due to uncertainties about the offset between the atmospheric CO_2 reservoir and that of intermediate waters in the Arctic Ocean, and the probable variations of this offset through time, in relation with sea ice cover and circulation patterns. Moreover, the ^{14}C ages likely correspond to short intervals of biogenic remain accumulation, when biogenic productivity was high enough to sustain zooplanktonic populations. Since detrital material is mostly transported by sea ice, the planktonic foraminifer populations analyzed at least partly originate from the "uploading" of suspended particulate matter over shelves, where first year ice forms and where productivity is much higher than in the central Arctic Ocean (Pabi et al., 2008). Consequently, the dated layers of foraminifers may represent populations mixed in time and space. In the context of the Arctic Ocean, relatively high biogenic productivity occurs during high sea levels episodes when shelves are submerged. This leads us to infer that productivity was probably discontinuous in time and that interpolations between dated layers may be misleading. In addition, the ^{210}Pb excess observed at MC-030 top ~2 cm matches ^{14}C ages of ~7,700 years (supporting information Tables S2 and S4), thus indicating that some shallow but effective benthic mixing occurs during high productivity intervals.

4.2. U Behavior in the Sedimentary Sequence

Calculating excesses in ^{231}Pa and ^{230}Th requires a clear understanding of U behavior in the sediment as diagenetic U-losses or gains would result in apparent excesses in these isotopes unrelated to initial fluxes of these isotopes from water column production. Here, several elements suggest that such diagenetic effects are not important. On one hand, the sequence depicts very small variations in its U contents (with a mean value of 1.25 ± 0.17 dpm/g; $\pm 1\sigma$; cf. supporting information Table S3), and a quasi-constant ^{234}U/^{238}U activity ratio (0.950 ± 0.008; $\pm 1\sigma$; Figure 4). The small variations observed in U and Th concentrations downcore (Figures 3 and 4) mostly respond to lithological differences: finer sediment show slightly higher Th contents likely due to Th adsorption over fine particles during earlier weathering/alteration processes of terrigenous supplies, an enrichment carried into deep marine sediments (e.g., Plain et al., 2004). Later on, we will see that such intervals with finer sediments record more active sea-ice deposition.

On another hand, the nearly constant ^{234}U/^{238}U activity ratio (0.950 ± 0.008; $\pm 1\sigma$) seems curious as, assuming a relatively constant initial disequilibrium between the two isotopes, ^{234}U should progressively return to equilibrium with ^{238}U through time, thus show a lesser disequilibrium near core bottom. As a matter of fact, the ^{234}U/^{238}U activity ratio averages 0.956 ± 0.006 near core bottom ($\pm 1\sigma$; 19 lowermost samples), versus 0.957 ± 0.030, near core top ($\pm 1\sigma$; 19 top samples). Either, the sediments recorded a decreasing inherited disequilibrium toward the Present, or discrete U-losses with preferential departure of ^{234}U compensating ^{234}U in situ growth due to ^{238}U decay, and/or ^{234}U-losses toward pore water by α-recoil effect matching its production through ^{238}U decay. In this scenario, and under steady state conditions:

1. with $d^{234}U^*/dt \sim \lambda_{234} * {}^{234}U \sim \phi^{234}U \sim \phi^{238}U$

   where $d^{234}U^*$ is the in situ growth of ^{234}U, whereas $\phi^{234}U$ and $\phi^{238}U$ are the chemical losses in these isotopes (assuming a loss with secular equilibrium, i.e., a ^{234}U/^{238}U activity ratio ~1 in the uranium lost by the sediment), and λ_{234}, the decay constant of ^{234}U that governs primarily the return to equilibrium with ^{238}U ($\lambda_{234} \sim 2.82 \times 10^{-3}$ ka^{-1});
2. with the following mean ^{234}U activity: 1.19 ± 0.15 dpm/g (supporting information Table S3);
3. it comes that $\phi^{234}U \sim -3.35 \pm 0.38 \times 10^{-3}$ dpm/g ka; and, as one may expect some preferential departure of ^{234}U, the loss in ^{238}U should be $\leq -3.35 \pm 0.38 \times 10^{-3}$ dpm/g ka, i.e., a loss-rate $\leq 2.68 \pm 0.31‰$/ka.

Still, over the few hundreds of thousand years represented by the cored sequence, as documented below, this chemical loss would be unlikely under the boundary conditions set, as can be inferred from the relatively constant U content.

The other possibility evoked above, that of losses of ^{234}U by α-recoil from the sediment is a process relatively well documented (e.g., Baskaran, 2011), but poorly quantified, although Vallières (1997) has illustrated in sediments from the deep Labrador Sea, increasing ^{234}U-deficits (versus ^{238}U) in the oxidized layers of isotopic stages 2, 4, and 6, with ^{234}U-adition at their upper and lower boundaries with the interlayered reduced sediments, but without any noticeable impact on U concentrations. Some long-term evolution of $^{234}U/^{238}U$ activities in terrigenous material carried into the Artic basin through glacial/interglacial cycles cannot be discarded either. We are thus left with an open scenario for the observed relatively stable U content and steady ^{234}U deficit, although, matching the present observations to those of Vallières (1997), we are tempted to put the emphasis of some discrete losses of U strongly enriched in ^{234}U due to the α-recoil effect.

Nevertheless, whatever the detailed behavior of U in the cored sequence, on can discard any significant loss that would result in large errors when estimating ^{230}Th and ^{231}Pa excesses versus their initial supported fractions in the sediment, as further discussed below.

4.3. Calculating ^{231}Pa and ^{230}Th Excesses

As documented above, any significant departure of uranium would result in residual excesses in daughter ^{231}Pa and ^{230}Th versus secular equilibrium with parent isotopes, below depths estimated for the final collapse of the initial excess ($^{231}Pa_{xs}$ and $^{230}Th_{xs}$), linked to water column production and scavenging by the settling particles. On the contrary, $^{230}Th_{xs}$ does not point to any "residual" activity downcore K-030 (supporting information Table S3), and even shows some negative values, in particular when calculated against ^{234}U activity (supporting information Table S3), pointing to possible enhanced losses in ^{234}U as the concerned depths.). These observations lead us to discard any significant loss of U in the sequence and to consider excesses in ^{230}Th calculated against ^{234}U as "minimum values" whereas those calculated against ^{238}U as likely, if not maximum values.

Nevertheless, the AR($^{230}Th/^{234}U$) versus AR($^{230}Th/^{238}U$) relationship (supporting information Figure S3) comes as follows:

$$AR\left(^{230}Th/^{234}U\right) = [1.003 \pm 0.004] * AR\left(^{230}Th/^{238}U\right) + [0.07 \pm 0.01]$$

$R > 0.99$; uncertainties are at $\pm 1\ \sigma$ level

In practical terms, the remaining $^{230}Th_{xs}$ over ^{234}U of the y-intercept means that any age calculated versus ^{234}U would be about $\sim 8 \pm 1$ ka older than the ^{238}U-based age: an offset leading to use the more likely value based on ^{238}U activities for the calculation of the "extinction age" of $^{230}Th_{xs}$, as further documented below. These ^{238}U-based $^{230}Th_{xs}$ values are thus plotted in Figures 3 and 5. They illustrate a strong temporal variability in $^{230}Th_{xs}$, with episodes of intense scavenging and relatively fine particulate deposition, alternating with episodes of negligible $^{230}Th_{xs}$ but coarser sedimentation.

$^{231}Pa_{xs}$ shows a faster decay downcore, of course, but similar large amplitude variability in its fluxes. As for $^{230}Th_{xs}$ some over-estimation of its "extinction" depth downcore may be assumed, due to possible U-losses. In core K-030, samples with AR($^{230}Th/^{234}U$) $\sim$ 1 yield a mean $^{230}Th/^{238}U$ ratio of 0.93 ± 0.03 ($\pm 1\sigma$). In the unlikely scenario in which this deficit in ^{230}Th would be exclusively linked to diagenetic (versus inherited) U-losses, the potential underestimation of the extinction age of $^{231}Pa_{xs}$ would be of the order of 3 ± 1.5 ka. This is within the analytical and calculation uncertainties of $^{231}Pa/^{235}U$ ratios leading to a $\pm 2\sigma$-age uncertainty of about ± 10 ka (supporting information Table S2).

For either $^{231}Pa_{xs}$ and $^{230}Th_{xs}$ final decay, the time limit can then be calculated as follows:

$$T_{lim.} = (1/\lambda) * \ln[A_{xs}/(2\sigma_p{}^2 + 2\sigma_d{}^2)^{0.5}]$$

where T_{lim} is the time limit (in ka), λ is the decay constant of the concerned isotope (ka^{-1}), A_{xs} is the core top (maximum) reference activity of the excess of this isotope, σ_p and σ_d are the error bars of parent (p) versus excess-daughter (d) isotope measurement or calculation, respectively; since $\sigma_p \ll \sigma_{d:}$

$$T_{lim.} \sim (1/\lambda) * \ln(A_{xs}/2\sigma_d{}^2).$$

This model is based on an approach proposed by Not and Hillaire-Marcel (2010): initial ^{230}Th and ^{231}Pa excesses in the sediment are considered approximately constant during intervals of fine sediment accumulation, thus follow a more or less exponential decay pattern, as illustrated Figures 3 and 4. This assumption is supported by similar "acceleration" trends between sediment accumulation and the decay-corrected $^{230}Th_{xs}$ cumulative curve in the ^{14}C-dated section of MC-030 (Figure 2b). Moreover, in Hoffmann and others' (2013) neither ours' here (Figure 2), show evidence for any missing $^{230}Th_{xs}$. On the contrary, excesses over water column production are observed during episodes of intense scavenging. Later on, we will show that inventories of $^{230}Th_{xs}$ are similar in remote sites (Mendeleev versus Lomonosov Ridges) and distinct depths (~1.3 to 2.5 km). This also leads to expect initial $^{230}Th_{xs}$ and $^{231}Pa_{xs}$ of similar magnitude during past intervals of intense scavenging. Inasmuch as it is not intended to interpolate ages for the setting of a continuous age model in the core, using such data, some variability in the initial $^{230}Th_{xs}$ and $^{231}Pa_{xs}$ should not drastically modify estimates of their extinction ages (i.e., about 5 half-lives of the concerned isotope in a first approximation).

As illustrated in Figure 3, $^{231}Pa_{xs}$ and $^{230}Th_{xs}$ fall below the $2\sigma_d$-threshold at depths of ~65 and ~125 cm, with benchmark age limits or "excess extinction ages," of about 140 and 300 ka, respectively. These benchmark ages and the radiocarbon-dated sequence point to a consistent mean sedimentation rate during the last glacial/interglacial cycles, despite the documented high frequency gaps in sedimentation, with values varying between 0.4 cm/ka (last 40 cal ka BP; Figure 2), 0.5 cm/ka (last ~140 ka; Figure 3), and 0.45 cm/ka (last ~300 ka, Figure 3).

4.4. Distribution and Decay of ^{230}Th-Excesses in Cores From Site PS87/30

Excesses in ^{230}Th are mostly restricted to short-duration episodes with ice-rafted deposition characterized by lesser proportions of coarse fractions (sand < 15%; Figure 3), thus likely linked to sea ice rather than to iceberg drifting. Nonetheless, when corrected for radioactive decay using the ^{14}C-calibrated age model, the $^{230}Th_{xs}$-inventory of the last ~40 ka sums up significantly above the vertical production in the overlying water column during the whole interval: ~210 dpm versus 115 dpm/cm^2 (Figure 2b). As this interval includes sedimentary gaps, in particular during most of the Holocene and the last glacial maximum, the budget and cycling of ^{230}Th in the central Arctic Ocean in relation to the sea ice and sedimentation histories seems unusual. ^{230}Th export from the Arctic Ocean through Fram Strait may have occurred during sediment "starvation" periods, but so far, evidence is missing, as highlighted above (Hoffmann & McManus, 2007) and further demonstrated here.

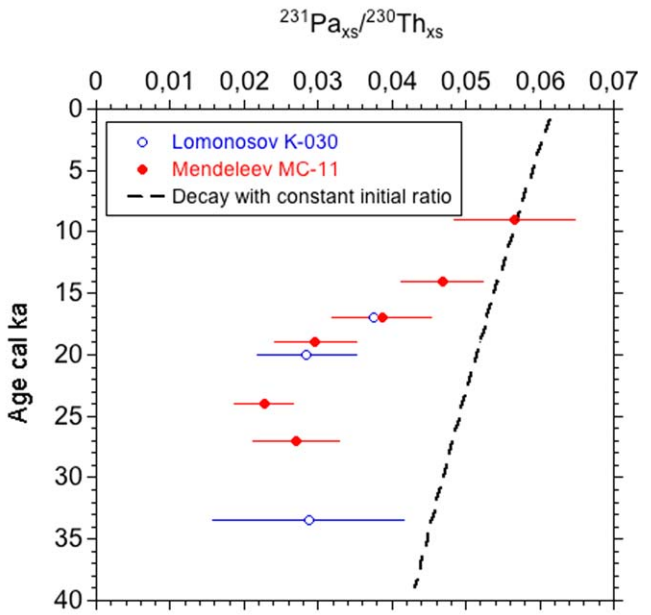

Figure 6. Temporal evolution of AR (^{231}Paxs/^{230}Thxs) downcore K-030 (composite sequence of Lomonosov; see supporting information) and in core MC-11 from Mendeleev Ridge (data from supporting information in Not and Hillaire-Marcel (2010)). The dotted curve illustrates the behavior expected for sediments characterized by initial constant excess ratio between these isotopes. This decrease of the initial ratio, back in time, has been documented by Hoffmann et al. (2013) for several sites of the Arctic Ocean.

4.5. ^{231}Pa-^{230}Th Fractionation

To a large extent, the $^{231}Pa_{xs}$ distribution downcore shows analogy with that of $^{230}Th_{xs}$, notably with respect to its linkage with sedimentary fluxes and reduced coarse fraction contents at the site (see also Moran et al., 2005). It differs by its faster decay rate and younger "extinction age." However, near the core top, from 0 to ~20 ^{14}C ka, where $^{231}Pa_{xs}$ measurements are sufficiently precise to be compared with those of $^{230}Th_{xs}$ (Figure 6), the $^{231}Pa_{xs}/^{230}Th_{xs}$ activity ratio decreases back in time much faster than expected given a constant initial ratio. One must therefore infer some fractionation between Pa and Th, much enhanced back in time, with a preferential export of ^{231}Pa likely toward subarctic seas, as previously documented by Hoffmann et al. (2013). These isotopes are strongly sensitive to the nature of the particulate fluxes responsible for their scavenging, notably the relative fluxes of carbonates and opal from diatom production (e.g., Baskaran, 2001; Chase et al., 2002; Siddal et al., 2005). Attempts at estimating the effect of these large-scale processes have been made (e.g., Edmonds et al., 2004; Moran et al., 2005; Trimble et al., 2004). A

scavenging model of these isotopes under the present boundary conditions has also been proposed at the scale of the Arctic Ocean (Luo & Lippold, 2015). We show below that brine spreading into the Arctic Ocean, as a consequence of sea-ice growth, may play a specific role in the cycling of these isotopes. Meanwhile, one can only concur with Moran and other's conclusion (2005): "while significant boundary scavenging of both ^{231}Pa and ^{230}Th occurs in the Arctic, there is a distinct lack of basin-margin fractionation [but] a sizable export of ^{231}Pa."

4.6. Correlation With Cores From the Mendeleev Ridge

Not and Hillaire-Marcel (2010) performed U-series isotope analysis in two multicores and the top section of a trigger weight core raised from the Northern Mendeleev Ridge (Figure 1): MC-11 (HLY-057-11, 83 07.730°N, 174 41.570°W, 2,570 m water depth), MC-12 (HLY-057-12, 83 17.797°N, 171 54.994°W, 1,586 m water depth), and TWC-11 (HLY-057-11, 83 08.615°N, 174 32.231°W, 2,644 m water depth) (see Polyak et al. (2009) and Kaufman et al. (2008) for sedimentological information about these cores). Despite a more than 1 km bathymetric difference between MC-11 and MC-12, these cores depict very similar $^{230}Th_{xs}$ and $^{210}Pb_{xs}$ profiles and inventories, raising further questions about the cycling of $^{230}Th_{xs}$ and $^{210}Pb_{xs}$ in the central Arctic Ocean since one would expect higher fluxes of both isotopes at the deeper site.

^{231}Pa measurements were also performed in MC-11, allowing some comparison with the Lomonosov sequence. The AR($^{231}Pa_{xs}/^{230}Th_{xs}$) ratios near core top at both sites (from 0.04 to 0.06; supporting information Table S3 and Not and Hillaire-Marcel (2010)) are in the range of values reported in earlier studies by Moran et al. (2005) and modeled by Luo and Lippold (2015), but in the lower range of values when compared with data in Hoffmann et al. (2013). As a few centimeters are missing on top of the shallower core K-030 from Lomonosov, ^{231}Pa and ^{230}Th excesses in its Holocene section are unconstrained. However, when plotted against their respective calibrated ^{14}C time scales, data from both MC-11 and K-030 seem tightly correlated through time (Figure 4). These data support inferences about lower initial ratios of $^{231}Pa_{xs}/^{230}Th_{xs}$ back in time, but do not support a bathymetric control, thus seem more in accordance with observations from Moran et al. (2005) than with Hoffmann et al. (2013).

As illustrated Figure 5, the $^{230}Th_{xs}$ profiles over both ridges are very similar, but for a deeper "extinction age" in the Lomonosov K-030 core (~125 cm) than that in the Mendeleev sequence (~38 cm in both MC-11 and MC-12). Similarly, ^{231}Pa data show a deeper "extinction age" in K-030 (~65 cm) than in MC-11 (~27 cm). These data, as well as the available ^{14}C-age control near core tops, point to mean sedimentation rates of ~4.3 mm/ka (Lomonosov) versus 1.7 mm/ka (Mendeleev), which yields a mean accumulation rate over Lomonosov of about 3-fold over that of the Mendeleev sites. At last, also based on the decay of $^{230}Th_{xs}$ in sedimentary cores from the southern Mendeleev Ridge, Gusev et al. (2013) calculated sedimentation rates not unlike those of MC-11 and MC-12 from the northern area of the ridge.

At this stage, a summary of the most robust features of $^{230}Th_{xs}$ behavior in sediments from the central Arctic Ocean can be made:

1. $^{230}Th_{xs}$-fluxes and inventories are similar in the Mendeleev and Lomonosov cores examined above (Figure 5), likely in several other sites of the central Arctic Ocean (Gusev et al., 2013; Huh et al., 1997; Moran et al., 2005) and seem thus independent of the site within this area.
2. $^{230}Th_{xs}$-fluxes and inventories are independent of the depth of the water column within the range documented here, i.e., from ~1.2 km (Mendeleev MC-12; Lomonosov-030) to ~2.5 km (Mendeleev MC-11); thus ^{230}Th-scavenging has to occur mostly outside the overlying water column and/or through a still undocumented process.
3. If $^{230}Th_{xs}$-fluxes vary in accordance with sediment fluxes (cf. Figure 2b), $^{230}Th_{xs}$-inventories are independent of the sediment accumulation as illustrated by their similarity in cores from both Mendeleev and Lomonosov (MC-11, Mc-030, and K-030) (Figure 5), notwithstanding a 3-fold difference in the sediment accumulation rate between the two ridges.

These observations lead to the following inferences:

1. Scavenging of ^{230}Th likely occurs over shelf "sea-ice factories," through multiple cycles of sediment resuspension, prior to sea ice uploading and transport toward ridges, as suggested for ^{210}Pb (Baskaran, 2005; see also Edmonds et al., 2004). In practical terms, intervals with efficient ^{230}Th-scavenging would

be associated with high relative sea levels when shelves are mostly submerged, notably in the Laptev-East Siberian Seas "sea-ice factories" (Reimnitz et al., 1994), thus making available fine sediment to be carried by sea ice, fostering sediment accumulation over ridges (Figure 2b). Such intervals would differ from those with iceberg-transported coarser fractions (Figure 3), more likely linked to streaming along ice-sheet margins during low sea level glacial episodes.

2. The similarity of $^{230}Th_{xs}$ and sediment accumulation profiles over Mendeleev sites MC-11 and MC-12 (Not & Hillaire-Marcel, 2010), two sites with a depth difference of more than 1 km, added to the fact that ^{230}Th fluxes are independent of sediment accumulation rates and of the specific ridge examined (Northern Lomonosov versus Mendeleev), both suggest that a mechanism other than fine sediment fractions scavenging, has also to be involved. One important feature of the Arctic Ocean during high sea level episodes and intense sea-ice production over shelves, is the corresponding release of brines linked to the closure of pores in sea ice (Golden et al., 2007). High-density brines (with salinity as high as 140 in Arctic sea ice (Not et al., 2012)) are likely to sink into the deep Arctic Ocean over shelf-edges. They also contain high concentrations or biological remains and colloidal/dissolved organic carbon (Thomas et al., 2008) with strong affinities with elements such as Th (e.g., Roy-Barman et al., 2005). These brines are more evenly spread into the central Arctic than sediments. We hypothesize here that they may the "joker" largely responsible for even ^{230}Th fluxes over ridges, whatever the bathymetry, at least down to ~2.5 km.

At first sight, ^{231}Pa shows analogies with ^{230}Th with respect to its relatively even distribution in the Mendeleev versus Lomonosov cores. It might thus be also dependent upon brine spreading mechanisms. However, its fractionation versus ^{230}Th, back in time (supporting information Figure S4; Hoffmann et al., 2013), demonstrates that other parameters also govern its cycling in the Arctic Ocean. As ^{231}Pa is highly sensitive to biogenic opal production (e.g., Venchiarutti et al., 2011), contrary to ^{230}Th (e.g., Roy-Barman et al., 2005), it should be closely related to diatom productivity, which depends upon Si-availability in the Arctic Ocean and is thus largely controlled by Si-fluxes from the northern Pacific Ocean when Bering Strait is open (e.g., Anderson et al., 1983).

4.7. Paleoceanographic Implications

The first outcome of the present study on Lomonosov Ridge and that of Not and Hillaire-Marcel (2010) or Gusev et al. (2013) on the Mendeleev Ridge, concerns the chronostratigraphy of late Quaternary sediment in the central Arctic Ocean. Both data sets point to significantly lower sedimentation rates than those reported in the recent literature. Whereas the chronology presented herein is in agreement with overall estimates by Clark et al. (1980) and most authors who published in the 80s and 90s, the recent literature often refers to a "consensual" chronological scheme based on an array of arguments for correlation across the Arctic Ocean, in particular on the presence of a layer characterized by abundant *Bulimina aculeata* in benthic foraminiferal assemblages. In the study core K-030 the *B. aculeata* layer is found at a depth of 70–90 cm (Stein, 2015), which corresponds to an interval falling between the extinction ages of $^{231}Pa_{xs}$ (~140 ka) and $^{230}Thxs$ (~300 ka). As discussed above, interpolated ages would be misleading. Nevertheless, assuming that fine particle accumulation corresponds to deglacial terminations and subsequent interglacials, the base of the *B. aculeata* layer would be associated with the marine isotope stage 8/7 transition and early stage 7. This not incompatible with an age of about 300 ka proposed originally for this layer by Ishman et al. (1996). However, a much younger age (marine isotope substage 5a) has been assigned to this horizon in more recent papers (Adler et al., 2009; Nørgaard-Pedersen et al., 2003; Polyak et al., 2004, 2013), using the chronological scheme of Jakobsson et al. (2000, 2001), which was mostly based on paleomagnetic excursion and color/manganese-rich layers counting. In the case of the paleomagnetic records, the investigations by Xuan and Channell (2010) on the Mendeleev Ridge and Xuan et al. (2012) on the Lomonosov Ridge raise serious concerns about the origin of the features interpreted as excursions. In the case of the color-based cyclostratigraphy related to manganese cycling, several works now tend to invalidate the assignment of Mn-rich layers to given intervals aside invalidating remote correlation of such layers at the scale of the Arctic Ocean (e.g., Macdonald & Gobeil, 2011; Meinhardt et al., 2016; Sundby et al., 2015). So far, the benchmark ages derived from the decay of excesses in ^{231}Pa and ^{230}Th provide the most reliable radiochronological benchmarks, fully in agreement with information from ^{14}C dating of core tops.

A striking feature arising from the comparison of the Mendeleev Ridge and Lomonosov Ridge cores is their large difference in sedimentation rates. The Lomonosov Ridge is located below the transpolar drift that

carries fine particulate material from the large Russian shelves, in particular the east Siberian and Laptev seas where sea ice forms annually. In comparison, the Mendeleev Ridge is fed by sediment carried by sea ice of the Beaufort gyre originating mostly from the narrow shelf of the Beaufort Sea. This leads to a 3-fold difference in their relative sedimentary accumulation rates (Figure 5).

Intervals with a higher coarse fraction content show reduced ^{230}Th excesses, likely in response to more important supplies from iceberg drifting and/or correspond to episodes of low sea level with emerged shelves and reduced sea-ice production. Whatever the cause, the low ^{230}Th excesses of such intervals suggest their short duration. In addition, sedimentary gaps might also occur during glacial stages in relation to the spreading of ice shelves. The ^{14}C-chronostratigraphic gap of the last glacial maximum illustrates such a situation (cf. also Polyak et al., 2004).

5. Conclusions

The present study adds credibility to the methodological approach outlined by Somayajulu et al. (1989), further developed by Not and Hillaire-Marcel (2010) and recently applied by Gusev et al. (2013) for the setting of radiometric benchmark ages of ~140 and ~300 ka based on the extinction of excesses in ^{231}Pa and ^{230}Th, respectively, in low sedimentation rate environments. In the case of the northern Lomonosov and Mendeleev Ridge, this approach suggests average sedimentation rates of the order of 4.3 and 1.7 mm/ka, respectively, during the late Quaternary. However, some caution is necessary when interpolating these values over shorter time intervals, as large amplitude changes occurred in the Arctic Ocean between glacial and interglacial or interstadial stages with respect to sedimentary regimes, sea ice history, continental ice streaming and sea level changes. The ^{14}C and U-series based chronologies suggest enhanced sedimentation by sea-ice rafting when shelves were at least partly submerged, thus allowing sediment uploading and transport by sea ice. Terminations with rapid sea level rise and continental ice melting seem to provide suitable conditions for relatively high sedimentation rates. In contrast, reduced deposition over ridges occurred during glacial episodes characterized by reduced shelves, although iceberg drifting linked to glacier ice surging occurred during such episodes. Still unexplained is the similarity of fluxes of ^{230}Th and ^{231}Pa linked to water column production, despite large differences in bathymetry and sedimentation rates of the central Arctic sites documented so far. The role of sea ice formation leading to regional brine production and spreading into the deep Arctic Ocean might be effective but should be documented further. The present study leads to suggest serious reconsideration of current chronological interpretations of Arctic stratigraphies in reference to open marine isotopic stages. Thus, so far, the role of the Arctic Ocean in the global paleoceanographic and paleoclimate system remains open to debate.

Acknowledgments
This study is a contribution to the Germany-Canada ArcTrain program. Financial support from NSERC-Canada to ArcTrain and NSERC-Discovery grants to chm and AdV were critical. Thanks are also due to Michel Preda (Department of Earth and Atmospheric Sciences, UQAM), for X-ray mineralogical analysis, and to Jens Matthiessen and Mike Zwick (Univ. Bremen), for their help with cores 030 sampling. All data used in the present paper are available in supporting information tables.

References

Adler, R. E., Polyak, L., Ortiz, J. D., Kaufman, D. S., Channell, J. E. T., Xuan, C.,. . . Crawford, K. A. (2009). Sediment record from the western Arctic Ocean with an improved Late Quaternary age resolution: HOTRAX core HLY0503-8JPC, Mendeleev Ridge. *Global and Planetary Change*, *68*(1–2), 18–29.

Aksu, A. E., & Mudie, P. J. (1985). Magnetostratigraphy and palynology demonstrate at least 4 million years of Arctic Ocean sedimentation. *Nature*, *318*(6043), 280–283.

Anderson, L. G., Dyrssen, D. W., Jones, E. P., & Lowings, M. G. (1983). Inputs and outputs of salt, fresh water, alkalinity, and silica in the Arctic Ocean. *Deep Sea Research, Part A*, *30*(1), 87–94.

Backman, J., Jakobsson, M., Løvlie, R., Polyak, L., & Febo, L. A. (2004). Is the central Arctic Ocean a sediment starved basin? *Quaternary Science Reviews*, *23*(11–13), 1435–1454.

Bacon, M. P., Huh, C. A., & Moore, R. M. (1989). Vertical profiles of some natural radionuclides over the Alpha Ridge, Arctic Ocean. *Earth and Planetary Science Letters*, *95*(1–2), 15–22.

Baskaran, M. (2001). Scavenging of thorium isotopes in the Arctic regions: Implications for the fate of particle-reactive pollutants. *Marine Pollution Bulletin*, *42*(1), 16–22.

Baskaran, M. (2005). Interaction of sea ice sediments and surface sea water in the Arctic Ocean: Evidence from excess ^{210}Pb. *Geophysical Research Letters*, *32*, L12601. https://doi.org/10.1029/2004GL022191

Baskaran, M. (2011). *Handbook of environmental isotope geochemistry* (951 p.). Berlin, Springer.

Baskaran, M., & Naidu, A. S. (1995). ^{210}Pb-derived chronology and the fluxes of ^{210}Pb and ^{137}Cs isotopes into continental shelf sediments, east Chukchi Sea, Alaskan Arctic. *Geochimica et Cosmochimica Acta*, 5, 4435–4448.

Bischof, J., Clark, D. L., & Vincent, J. S. (1996). Origin of ice-rafted debris: Pleistocene paleoceanography in the western Arctic Ocean. *Paleoceanography*, *11*(6), 743–756.

Blaauw, M., & Christen, J. A. (2011). Flexible paleoclimate age-depth models using an autoregressive gamma process. *Bayesian Analysis*, *6*, 457–474.

Blott, S. J., & Pye, K. (2001). Gradistat: A grain size distribution and statistics package for the analysis of unconsolidated sediments. *Earth Surface Processes and Landforms*, *26*, 1237–1248.

Chase, Z., Anderson, R. F., Fleisher, M. Q., & Kubik, P. W. (2002). The influence of particle composition and particle flux on scavenging of Th, Pa and Be in the ocean. *Earth and Planetary Science Letters*, *204*(1–2), 215–229.
Cheng, H., Edwards, R. L., Hoff, J., Gallup, C. D., Richards, D. A., & Asmerom, Y. (2000). The half-lives of uranium-234 and thorium-230. *Chemical Geology*, *169*(1–2), 17–33.
Clark, D. L., Whitman, R. R., Morgan, K. A., & Mackey, S. D. (1980). Stratigraphy and glacial-marine sediments of the Amerasian Basin, central Arctic Ocean. In *Special paper of the Geological Society of America* (pp. 1–57).
CliC/AMAP/IASC (2016). *The arctic freshwater system in a changing climate. WCRP Climate and Cryosphere (CliC) project*. Arctic Monitoring and Assessment Programme (AMAP), International Arctic Science Committee (IASC).
Cochran, K. J., Hirschberg, D. J., Livingston, H. D., Buesseler, K. O., & Key, R. M. (1995). Natural and anthropogenic radionuclide distributions in the Nansen Basin, Artic Ocean: Scavenging rates and circulation timescales. *Deep Sea Research, Part II*, *42*(6), 1495–1517.
Cronin, T. M., DeNinno, L. H., Polyak, L., Caverly, E. K., Poore, R. Z., Brenner, A.,. . . Marzen, R. E. (2014). Quaternary ostracode and foraminiferal biostratigraphy and paleoceanography in the western Arctic Ocean. *Marine Micropaleontology*, *111*, 118–133.
Darby, D. A., Bischof, J. F., Spielhagen, R. F., Marshall, S. A., & Herman, S. W. (2002). Arctic ice export events and their potential impact on global climate during the late Pleistocene. *Paleoceanography*, *17*(2), https://doi.org/10.1029/2001PA000639
DePaolo, D. J., Maher, K., Christensen, J., & McManus, J. F. (2006). Sediment transport time measured with U-series isotopes: Results from ODP North Atlantic drift site 984. *Earth and Planetary Science Letters*, *248*, 394–410.
Edmonds, H. N., Moran, S. B., Cheng, H., & Edwards, R. L. (2004). ^{230}Th and ^{231}Pa in the Arctic Ocean: Implications for particle fluxes and basin-scale Th/Pa fractionation. *Earth and Planetary Science Letters*, *227*(1–2), 155–167.
Fleisher, M. Q., & Anderson, R. F. (2003). Assessing the collection efficiency of Ross Sea sediment traps using ^{230}Th and ^{231}Pa. *Deep Sea Research, Part II*, *50*, 693–712.
Golden, K. M., Eicken, H., Heaton, A. L., Miner, J., Pringle, D. J., & Zhu, J. (2007). Thermal evolution of permeability and microstructure in sea ice. *Geophysical Research Letters*, *34*, L16501. https://doi.org/10.1029/2007GL030447
Guo, L., Chen, M., & Gueguen, C. (2002). Control of Pa/Th ratio by particulate chemical composition in the ocean. *Geophysical Research Letters*, *29*(20), 1961. https://doi.org/10.1029/2002GL015666
Gusev, E. A., Maksimov, F. E., Yu. Kuznetsov, V., Basov, V. A., Novikhina, E. S., Kupriyanova, N. V.,. . . Zherebtsov, I. E. (2013). Stratigraphy of bottom sediments in the Mendeleev Ridge Area (Arctic Ocean). *Doklady Earth Sciences*, *450*, 602–606.
Hanslik, D., Jakobsson, M., Backman, J., Björck, S., Sellén, E., O'Regan, M.,. . . Skog, G. (2010). Quaternary Arctic Ocean sea ice variations and radiocarbon reservoir age corrections. *Quaternary Science Reviews*, *29*, 3430–3441.
Hiess, J., Daniel, J. C., McLean, N., & Noble, S. R. (2012). ^{235}U/^{238}U systematics in terrestrial uranium-bearing minerals. *Science*, *335*, 1610–1614.
Hoffmann, S., & McManus, J. (2007). Is there a ^{230}Th deficit in Arctic sediments? *Earth and Planetary Science Letters*, *258*(3–4), 516–527.
Hoffmann, S. S., McManus, J. F., Curry, W. B., & Susan Brown-Leger, L. (2013). Persistent export of ^{231}Pa from the deep central Arctic Ocean over the past 35,000 years. *Nature*, *497*(7451), 603–606.
Huh, C. A., Pisias, N. G., Kelley, J. M., Maiti, T. C., & Grantz, A. (1997). Natural radionuclides and plutonium in sediments from the western Arctic Ocean: Sedimentation rates and pathways of radionuclides. *Deep Sea Research, Part II*, *44*(8), 1725–1743.
Ishman, S. E., Polyak, L., & Poore, R. Z. (1996). An expanded record of Pleistocene deep Arctic change: Canada Basin, western Arctic Ocean. *Geology*, *24*, 139–142.
Jakobsson, M., Backman, J., Murray, A., & Løvlie, R. (2003). Optically stimulated luminescence dating supports central Arctic Ocean cm-scale sedimentation rates. *Geochemistry, Geophysics, Geosystems*, *4*(2), 1016. https://doi.org/10.1029/2002GC000423
Jakobsson, M., Lovlie, R., Al-Hanbali, H., Arnold, E., Backman, J., & Rth, M. M. (2000). Manganese and color cycles in Arctic Ocean sediments constrain Pleistocene chronology. *Geology*, *28*(1), 23–26.
Jakobsson, M., Løvlie, R., Arnold, E. M., Backman, J., Polyak, L., Knutsen, J. O., & Musatov, E. (2001). Pleistocene stratigraphy and paleoenvironmental variation from Lomonosov Ridge sediments, central Arctic Ocean. *Global and Planetary Change*, *31*(1–4), 1–22.
Jakobsson, M., Mayer, L., Coakley, B., Dowdeswell, J. A., Forbes, S., Fridman, B., . . . Weatherall, P. (2012). The International Bathymetric Chart of the Arctic Ocean (IBCAO) Version 3.0. *Geophysical Research Letters*, *39*. https://doi.org/10.1029/2012GL052219
Kaufman, D. S., Polyak, L., Adler, R., Channell, J. E. T., & Xuan, C. (2008). Dating late Quaternary planktonic foraminifer *Neogloboquadrina pachyderma* from the Arctic Ocean using amino acid racemization. *Paleoceanography*, *23*, PA3224. https://doi.org/10.1029/2008PA001618
Kraus, K. A., Moore, G. E., & Nelson, F. (1956). Anion-exchange Studies. XXI. Th(IV) and U(IV) in hydrochloric acid. Separation of thorium, protactinium and uranium. *Journal of the American Chemical Society*, *78*, 2692–2695.
Ku, T. L., & Broecker, W. S. (1965). Rates of sedimentation in the Arctic Ocean. *Progress in Oceanography*, *4*, 95–104.
Löwemark, L., März, C., O'Regan, M., & Gyllencreutz, R. (2014). Arctic Ocean Mn-stratigraphy: Genesis, synthesis and inter-basin correlation. *Quaternary Science Reviews*, *92*, 97–111.
Luo, Y., & Lippold, J. (2015). Controls on ^{231}Pa and ^{230}Th in the Arctic Ocean. *Geophysical Research Letters*, *42*, 5942–5949. https://doi.org/10.1002/2015GL064671
Macdonald, R. W., & Gobeil, C. (2011). Manganese sources and sinks in the Arctic Ocean with reference to periodic enrichments in basin sediments. *Aquatic Geochemistry*, *18*(6), 565–591.
Martín-Ramos, J. D., Díaz-Hernández, J., Cambeses, L. A., Scarrow, J. H., & López-Galindo, A. (2012). *Pathways for quantitative analysis by x-ray diffraction: An introduction to the study of mineralogy* (154 p.). Rijeka, Croatia: Intech Europe.
Meinhardt, A. K., März, C., Schuth, S., Lettmann, K. A., Schnetger, B., Wolff, J. O., & Brumsack, H. J. (2016). Diagenetic regimes in Arctic Ocean sediments: Implications for sediment geochemistry and core correlation. *Geochimica et Cosmochimica Acta*, *188*, 125–146.
Moran, S. B., Shen, C. C., Edwards, R. L., Edmonds, H. N., Scholten, J. C., Smith, J. N., & Ku, T. L. (2005). ^{231}Pa and ^{230}Th in surface sediments of the Arctic Ocean: Implications for ^{231}Pa/^{230}Th fractionation, boundary scavenging, and advective export. *Earth and Planetary Science Letters*, *234*(1–2), 235–248.
Nørgaard-Pedersen, N., Spielhagen, R. F., Erlenkeuser, H., Grootes, P. M., Heinemeier, J., & Knies, J. (2003). Arctic Ocean during the Last Glacial Maximum: Atlantic and polar domains of surface water mass distribution and ice cover. *Paleoceanography*, *18*(3), 1063. https://doi.org/10.1029/2002PA000781
Not, C., & Hillaire-Marcel, C. (2010). Time constraints from ^{230}Th and ^{231}Pa data in late Quaternary, low sedimentation rate sequences from the Arctic Ocean: An example from the northern Mendeleev Ridge. *Quaternary Science Reviews*, *29*(25–26), 3665–3675.
Not, C., Brown, K., Ghaleb, B., & Hillaire-Marcel, C. (2012). Conservative behavior of uranium vs. salinity in Arctic sea ice and brine. *Marine Chemistry*, *130–131*, 33–39.
Not, C., Hillaire-Marcel, C., Ghaleb, B., Polyak, L., & Darby, D. (2008). ^{210}Pb-^{226}Ra-^{230}Th systematics in very low sedimentation rate sediments from the Mendeleev Ridge (Arctic Ocean). *Canadian Journal of Earth Sciences*, *45*(11), 1207–1219.

O'Regan, M., King, J., Backman, J., Jakobsson, M., Pälike, H., Moran, K.,. . . Jordan, R. W. (2008). Constraints on the Pleistocene chronology of sediments from the Lomonosov Ridge. *Paleoceanography*, *23*, PA1S19. https://doi.org/10.1029/2007PA001551

Ovaskainen, R. (1999). *The determination of minor isotope abundances in naturally occurring uranium materials: The tracing power of isotopic signatures for uranium* (Rep. Ser. in Radiochemistry HY-RAD--12/1999). Finland.

Pabi, S., van Dijken, G. L., & Arrigo, K. R. (2008). Primary production in the Arctic Ocean, 1998–2006. *Journal of Geophysical Research*, *113*, C08005. https://doi.org/10.1029/2007JC004578

Plain, C., Hillaire-Marcel, C., & Ghaleb, B. (2004). Paleointensity of the western boundary undercurrent since the last glacial maximum from ^{230}Th excess-changes in deep Irminger Sea sediments. *Spring Meeting 2004* (Abstract #GC21A-04). Washington, DC: American Geophysical Union.

Polyak, L., Best, K. M., Crawford, K. A., Council, E. A., & St-Onge, G. (2013). Quaternary history of sea ice in the western Arctic Ocean based on foraminifera. *Quaternary Science Reviews*, *79*, 145–156.

Polyak, L., Bischof, J., Ortiz, J. D., Darby, D. A., Channell, J. E. T., Xuan, C.,. . . Council, E. A. (2009). Late Quaternary stratigraphy and sedimentation patterns in the western Arctic Ocean. *Global and Planetary Change*, *68*(1–2), 5–17.

Polyak, L., Curry, W. B., Darby, D. A., Bischof, J., & Cronin, T. M. (2004). Contrasting glacial/interglacial regimes in the western Arctic Ocean as exemplified by a sedimentary record from the Mendeleev Ridge. *Palaeogeography, Palaeoclimatology, Palaeoecology*, *203*(1–2), 73–93.

Pons-Branchu, E., Hillaire-Marcel, C., Deschamps, P., Ghaleb, B., and D. J. Sinclair (2005), Early diagenesis impact on precise U-series dating of deep-sea corals: Example of a 100–200-year old Lophelia pertusa sample from the northeast Atlantic, *Geochimica et Cosmochimica Acta*, *69*, 4865–4879.

Reimer, P. J., & Reimer, R. W. (2001). A marine reservoir correction database and on-line interface, *Radiocarbon*, *43*, 461–463.

Reimnitz, E., Dethleff, D., & Nürnberg, D. (1994). Contrasts in Arctic shelf sea-ice regimes and some implications: Beaufort Sea versus Laptev Sea. *Marine Geology*, *119*(3–4), 215–225.

Robert, J., Miranda, C. F., & Muxart, R. (1969). Mesure de la période du protactinium 231 par microcalorimétrie. *Radiochimica Acta*, *11*(2), 104–108.

Roy-Barman, M., Jeandel, Souhaut, C. M., van der Loeff, M., Voege, R., Leblond, I. N., & Freydier, R. (2005). The influence of particle composition on thorium scavenging in the NE Atlantic Ocean (POMME experiment). *Earth and Planetary Science Letters*, *240*(3–4), 681–693.

Scholten, J. C., Rutgers van der Loeff, M. M., & Michel, A. (1995). Distribution of ^{230}Th and ^{231}Pa in the water column in relation to the ventilation of the deep Arctic basins. *Deep Sea Research, Part II*, *42*(6), 1519–1531.

Sellén, E., Jakobsson, M., Frank, M., & Kubik, P. W. (2009). Pleistocene variations of beryllium isotopes in central Arctic Ocean sediment cores. *Global and Planetary Change*, *68*(1–2), 38–47.

Serreze, M. C., & Francis, J. A. (2006). The arctic amplification debate. *Climatic Change*, *76*(3–4), 241–264.

Siddall, M., Henderson, G. M., Edwards, N. R., Frank, M., Müller, S. A., Stocker, T. F., & Joos, F. (2005). ^{231}Pa/^{230}Th fractionation by ocean transport, biogenic particle flux and particle type. *Earth and Planetary Science Letters*, *237*(1–2), 135–155.

Somayajulu, B. L. K., Sharma, P., & Herman, Y. (1989). Thorium and uranium isotopes in Arctic sediments. *The Arctic Seas*, 571–579.

Stein, R. (2015). The expedition PS87 of the Research Vessel Polarstern to the Arctic Ocean in 2014, *Berichte zur Polar- und Meeresforschung = Reports on Polar and Marine Research*, *688*, 1–273.

Sundby, B., Lecroart, P., Anschutz, P., Katsev, S., & Mucci, A. (2015). When deep diagenesis in Arctic Ocean sediments compromises manganese-based geochronology. *Marine Geology*, *366*, 62–68.

Thomas, D. N., & Papadimitriou, S. (2008). Biogeochemistry of sea ice. In *Sea ice* (pp. 267–302). Hoboken, NJ: Blackwell Science Ltd.

Thorez, J. (2003). L'argile, mineral pluriel. *Bulletin de la Societe Royale des Sciences de Liege*, *72*(1), 19–70.

Trimble, S. M., Baskaran, M., & Porcelli, D. (2004). Scavenging of thorium isotopes in the Canada Basin of the Arctic Ocean. *Earth and Planetary Science Letters*, *222*(3–4), 915–932.

Venchiarutti, C., Roy-Barman, M., Freydier, R., Van Beek, P., Souhaut, M., & Jeandel, C. (2011). Influence of intense scavenging on Pa-Th fractionation in the wake of Kerguelen Island (Southern Ocean). *Biogeosciences*, *8*(11), 3187–3201.

Vallières, S. (1997). *Flux d'uranium et excès de ^{230}Th dans les sédiments de la mer du Labrador* (PhD thesis Université du Québec à Montréal, 130 p.)

Viers, J., Dupré, B., & Gaillardet, J. (2009). Chemical composition of suspended sediments in World Rivers: New insights from a new database. *Science of the Total Environment*, *407*(2), 853–868.

Xuan, C., & Channell, J. E. T. (2010). Origin of apparent magnetic excursions in deep-sea sediments from Mendeleev-Alpha Ridge, Arctic Ocean. *Geochemistry, Geophysics, Geosystems*, *11*, Q02003. https://doi.org/10.1029/2009GC002879

Xuan, C., Channell, J. E. T., Polyak, L., & Darby, D. A. (2012). Paleomagnetism of Quaternary sediments from Lomonosov Ridge and Yermak Plateau: Implications for age models in the Arctic Ocean. *Quaternary Science Reviews*, *32*, 48–63.

Zwick, M. M. (2016). *Reconstruction of water mass characteristics on the western Lomonosov Ridge (Central Arctic Ocean)* (MSc Memoir, 86 p.). Bremen, Germany: Bremen Universität.